LncPSCA in the 8q24.3 risk locus drives gastric cancer through destabilizing DDX5

Yan Zheng[1,2,3] iD, Tianshui Lei[2], Guangfu Jin[4], Haiyang Guo[5] iD, Nasha Zhang[6], Jie Chai[7], Mengyu Xie[2], Yeyang Xu[2], Tianpei Wang[4], Jiandong Liu[2], Yue Shen[2], Yemei Song[2], Bowen Wang[2], Jinming Yu[6,*] iD & Ming Yang[2,**] iD

Abstract

Genome-wide association studies (GWAS) have identified multiple gastric cancer risk loci and several protein-coding susceptibility genes. However, the role of long-noncoding RNAs (lncRNAs) transcribed from these risk loci in gastric cancer development and progression remains to be explored. Here, we functionally characterize a lncRNA, lncPSCA, as a novel tumor suppressor whose expression is fine-regulated by a gastric cancer risk-associated genetic variant. The rs2978980 T > G change in an intronic enhancer of *lncPSCA* interrupts binding of transcription factor RORA, which down-regulates lncPSCA expression in an allele-specific manner. LncPSCA interacts with DDX5 and promotes DDX5 degradation through ubiquitination. Increased expression of lncPSCA results in low levels of DDX5, less RNA polymerase II (Pol II) binding with DDX5 in the nucleus, thus activating transcription of multiple p53 signaling genes by Pol II. These findings highlight the importance of functionally annotating lncRNAs in GWAS risk loci and the great potential of modulating lncRNAs as innovative cancer therapy.

Introduction

According to the GLOBOCAN estimates, gastric cancer (GC) is the fifth most frequently diagnosed malignancy ($n = 1,089,103$ new cases, 5.6% of the total cancer cases) and the fourth leading cause of cancer death worldwide ($n = 768,793$ deaths, 7.7% of the total cancer deaths) in 2020 (Sung *et al*, 2021). Incidence rates of GC are markedly elevated in Eastern Asia including China. *H. pylori* infection, foods preserved by salting, low fruit intakes, alcohol consumption and active tobacco smoking are established risk factors for GC (Sung *et al*, 2021). Among them, *H. pylori* infection is predominantly important (Plummer *et al*, 2015). However, only a small portion of individuals infected by *H. pylori* eventually developed GC, elucidating that the genetic makeup also plays a crucial part in GC etiology.

Genome-wide association studies (GWASs) have identified multiple GC risk loci, such as 1q22, 1p35.2, 3q13.31, 3q11.2, 4q28.1, 5p13.1, 5q14.3, 6p21.1, 6p22.1, 8q24.3, 9q34.2, 10q23.33, 11q22.3, 12q24.11-12 and 20q11.21 (Sakamoto *et al*, 2008; Abnet *et al*, 2010; Saeki *et al*, 2011; Shi *et al*, 2011; Helgason *et al*, 2015; Hu *et al*, 2016; Wang *et al*, 2017; Zhu *et al*, 2017; Tanikawa *et al*, 2018; Yan *et al*, 2020). Several genes in these risk loci have been functionally confirmed as GC-susceptibility genes, including *MUC1* at 1q22 (Saeki *et al*, 2015), *SPOCD1* at 1p35.2 (Hu *et al*, 2016), *PSCA* at 8q24.3 (Sakamoto *et al*, 2008; Sung *et al*, 2016; Yan *et al*, 2020), *PRKAA1* at 5p13.1 (Yan *et al*, 2020), *BTN3A2* at 6p22.1 (Hu *et al*, 2016), and *NOC3L* at 10q23.33 (Yan *et al*, 2020). For example, down-regulation of *PSCA* at 8q24.3 was reported in GC specimens compared to normal tissues. Consistently, the growth efficiency of GC cells stably overexpressing PSCA was slower than that of GC cells with low PSCA expression, which supports its role as a tumor suppressor (Sakamoto *et al*, 2008). The GC-susceptibility rs2294008 T allele in *PSCA* 5'-UTR generates a consensus binding sequence for transcription factor Yin Yang 1 (YY1), recruits YY1 to *PSCA* promoter and significantly suppresses *PSCA* expression *in vivo*, which eventually predisposes gastric epithelial cells to GC development (Sakamoto *et al*, 2008; Saeki *et al*, 2015; Sung *et al*, 2016).

Long noncoding RNAs (lncRNAs) are a class of long transcripts which are more than 200 nucleotides and mostly cannot be translated into proteins (Leucci *et al*, 2016; Leucci, 2018; ICGC/TCGA

1 Research Center of Translational Medicine, Jinan Central Hospital Affiliated to Shandong First Medical University, Jinan, China
2 Shandong Provincial Key Laboratory of Radiation Oncology, Cancer Research Center, Shandong Cancer Hospital and Institute, Shandong First Medical University and Shandong Academy of Medical Sciences, Jinan, China
3 Jinan Central Hospital, Cheeloo College of Medicine, Shandong University, Jinan, China
4 Department of Epidemiology, Center for Global Health, School of Public Health, Nanjing Medical University, Nanjing, China
5 Clinical Laboratory, Tumor Marker Detection Engineering Laboratory of Shandong Province, The Second Hospital of Shandong University, Jinan, China
6 Department of Radiation Oncology, Shandong Cancer Hospital and Institute, Shandong First Medical University and Shandong Academy of Medical Sciences, Jinan, China
7 Department of Gastrointestinal Surgery, Shandong Cancer Hospital and Institute, Shandong First Medical University and Shandong Academy of Medical Sciences, Jinan, China
 *Corresponding author. Tel/Fax: +86 531 67626971; E-mail: sdyujinming@126.com
 **Corresponding author (lead contact). Tel/Fax: +86 531 67626536; E-mail: aaryoung@yeah.net

Pan-Cancer Analysis of Whole Genomes Consortium, 2020; Statello *et al*, 2021). Although originally considered as transcriptional noise of human genome, lncRNAs have been implicated in development of cancers with varying levels of evidences (Leucci, 2018; Statello *et al*, 2021). Recent studies indicated that several lncRNAs, which are transcribed from genome intervals surrounding cancer risk signals, are involved in tumorigenesis (Guo *et al*, 2016; Betts *et al*, 2017; Cho *et al*, 2018; Gao *et al*, 2018; Hua *et al*, 2018; Leucci, 2018; Moradi Marjaneh *et al*, 2020; Statello *et al*, 2021). However, the role of lncRNAs transcribed from the GC-susceptibility loci in disease development and progression remains to be explored.

In the current study, we fine-mapped the *PSCA* locus (chr8:143,757,626–143,758,499) in our previous meta-analysis of four Chinese ancestry GWASs, and found that one functional GC risk rs2978980 SNP located within an intronic enhancer of *lncPSCA* (NR_033343.1, the noncoding transcript of *PSCA*). Interestingly, the rs2978980 genetic variant interrupts binding of transcription factor RORA and regulates lncPSCA expression *in vivo* and *in vitro*. In particular, the protective T allele-activated lncPSCA suppresses GC proliferation and metastasis through interacting with DDX5 and reprogramming RNA polymerase II (RNA Pol II)-regulated transcriptional activation of downstream tumor suppressor genes.

Results

The SNP rs2978980 is located at a functional enhancer in the 8q24.3 GC-susceptibility locus

To identify functional GC-susceptibility SNPs in the 8q24.3 locus (chr8:143,749,715–143,766,143), we systematically evaluated seventy-five SNPs using our previous meta-GWASs including 3,771

GC cases and 5,426 controls from four Chinese ancestry datasets (Yan *et al*, 2020). Among these genetic polymorphisms, forty-two SNPs are significantly associated with GC risk after Bonferroni correction ($P < 6.7 \times 10^{-4}$), including rs2294008 and rs2976392 which were reported previously (Appendix Table S1; Sakamoto *et al*, 2008; Lochhead *et al*, 2011; Shi *et al*, 2011; Wang *et al*, 2012; Mocellin *et al*, 2015; Sung *et al*, 2016; Cui *et al*, 2019). Interestingly, two GC-risk SNPs rs2978980 and rs2920282, which are in complete linkage disequilibrium (LD) ($r^2 = 1$) are located in an enhancer region in gastric tissues according to the Roadmap Epigenomics and ENCODE projects (Fig 1A and Appendix Fig S1). Notably, *in situ* Hi-C assays indicated that the enhancer region is close to the transcription start site (TSS) of *lncPSCA*, but not the TSS of the protein-coding *PSCA* (GenBank: NM_005672.4), in 3D architecture of human genome (Appendix Fig S2; Rao *et al*, 2014), suggesting that it might be an intronic enhancer of *lncPSCA*. Transcription factor binding prediction indicated that the rs2978980 T allele shows transcription factor RORA binding but the G allele does not (Fig 1B). Consistent to our data in Chinese populations, the rs2978980 SNP was also significantly associated with GC risk in a European population-based on a GWAS including 2,500 population-based GC patients and 205,652 controls ($P = 1.7 \times 10^{-7}$; Helgason *et al*, 2015).

Since rs2978980 SNP is located in the RORA consensus binding sequence, we conducted electrophoretic mobility-shift assays (EMSA) to distinguish the differences in binding ability between the rs2978980T and G alleles to RORA (Fig 1C). We found that RORA-containing HGC-27 nuclear extracts bound only to the biotin-labeled oligonucleotide probe with the T allele or the RORA consensus sequence but not the G allele probe (Fig 1C). A 100-fold excess of unlabeled T allele oligonucleotides or unlabeled RORA consensus oligonucleotides efficiently competed for the binding activity of the T allele probe (Fig 1C). However, unlabeled G allele


Figure 1. Gastric cancer risk SNP rs2978980 alters the enhancer activity of a novel lncRNA *lncPSCA* in the 8q24 locus. ▶

A   A schematic view of the *lncPSCA* and *PSCA* loci. The risk-associated SNP rs2978980 is shown as the red vertical line. Data from the UCSC Genome Browser, including epigenetic marks for histone H3 lysine 27 acetylation (H3K27ac), are shown.

B   Abolishment of a RORA binding site in the *lncPSCA* intronic enhancer by the rs2978980 T > G SNP. The risk allele G of rs2978980 disrupts a RORA binding motif.

C   Electrophoretic mobility-shift assay (EMSA) with biotin-labeled RORA consensus, rs2978980T or rs2978980G probes and HGC-27 or MGC80-3 nuclear extracts. HGC-27 or MGC80-3 left panel: EMSA with RORA consensus or rs2978980T probes. Lane 1–8: from the first lane at the left side to the right side. Lanes 4 and 8, probe only; lanes 2 and 6, probe and nuclear extracts; lanes 1, 3, 5, and 7, probe and nuclear extracts plus 100× unlabeled rs2978980T (lanes 1 and 5) or RORA consensus probes (lanes 3 and 7). HGC-27 or MGC80-3 right panel: EMSA with rs2978980T or rs2978980G probes. Lanes 1 and 6, probe only; lanes 2 and 7, probe and nuclear extracts; lanes 3–5 and 8–10, probe and nuclear extracts plus 100× unlabeled rs2978980T (lanes 5 and 8), rs2978980G (lanes 3 and 10), or RORA consensus probes (lanes 4 and 9).

D   Sanger sequencing chromatograms of the SNP region indicated that the MGC80-3 cell line carries the TG genotype and HGC-27 has the GG genotype.

E   ChIP-qPCR assays using MGC80-3 cells carrying the rs2978980TG genotype. The presence of RORA-binding *lncPSCA* enhancer region was verified by qPCR with *NPAS2* as the positive control. Region a and b: the negative control regions of *lncPSCA* promoter and intron 1; region c: the *lncPSCA* enhancer region around rs2978980 SNP; region d: the positive control *NPAS2* promoter region. Left subpanel: RORA ChIP-qPCR fragments on *lncPSCA* (a, b, and c) and *NPAS2* (d) genes; right subpanel: RORA ChIP-qPCR results of *lncPSCA* (a, b, and c) and *NPAS2* (d) genes. Data show one representative example of three biological replicates.

F   Suppression of *RORA* using siRNAs (siRORA-1 and siRORA-2) could markedly down-regulate *lncPSCA* expression in MGC80-3 cells but not in HGC-27 cells. In details, MGC80-3 and HGC-27 cells were transfected with siRORA-1 and siRORA-2, *lncPSCA* and *RORA* expression levels were measured by RT–qPCR and Western blot.

G   In gastric cancer or normal tissues of discovery cohort (*n* = 96) and validation cohort (*n* = 30), there were significantly positive expression correlations between *RORA* and *lncPSCA*.

H   Expression levels of lncPSCA were quantified using RT–qPCR in tumor-normal pairs of both cohorts, respectively. All data of lncPSCA expression were normalized to *GAPDH* expression levels.

I   In gastric cancer or normal tissues of both cohorts, there was a significant allele-differential expression between rs2978980G-allele carriers or T-allele carriers.

Data information: The difference between two groups was calculated using Student's *t* test. One-way ANOVA analysis with Dunnett's test was used for multiple comparisons. The significance of association between gene expression and rs2978980 genotypes was calculated using Spearman's correlation. *$P < 0.05$; **$P < 0.01$; ***$P < 0.001$.
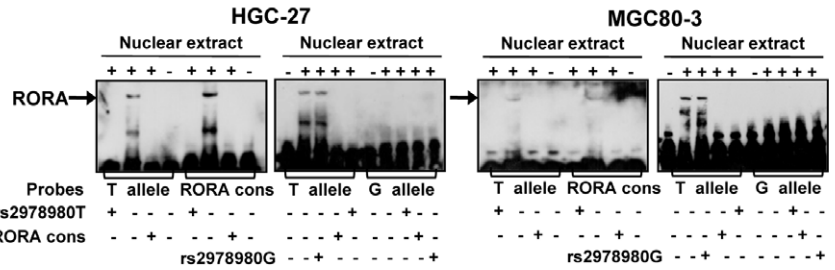
Source data are available online for this figure.
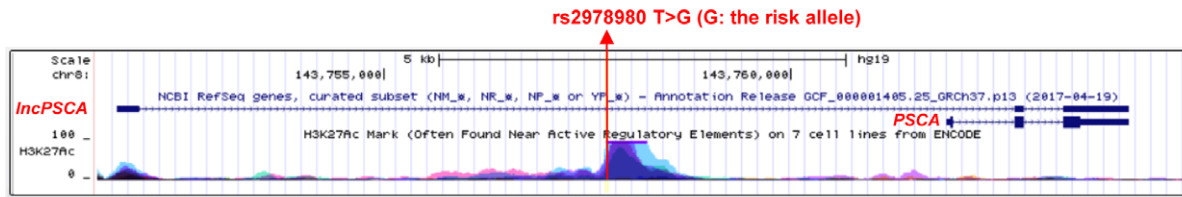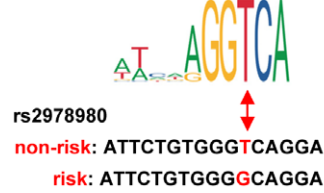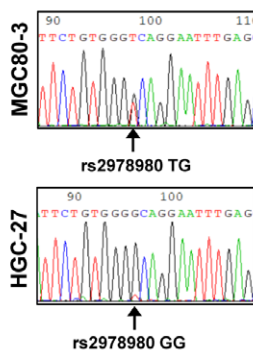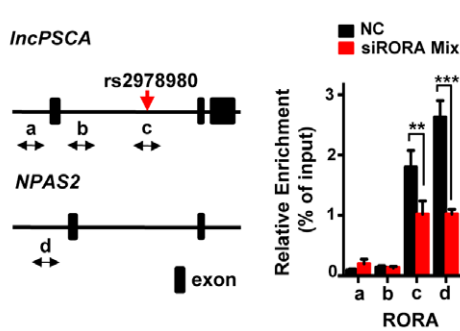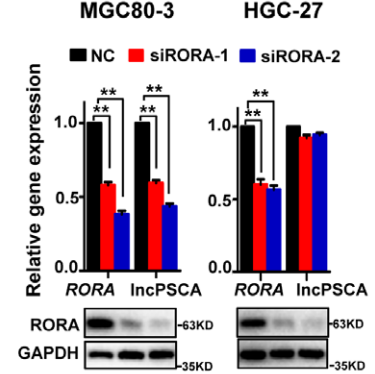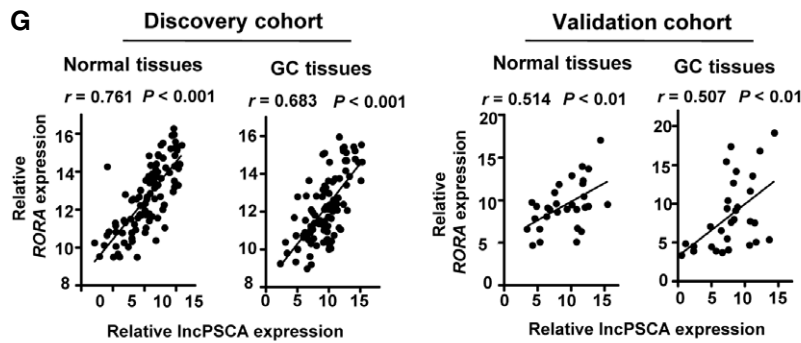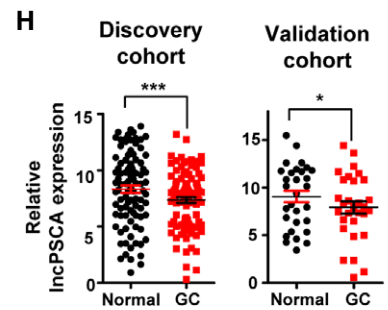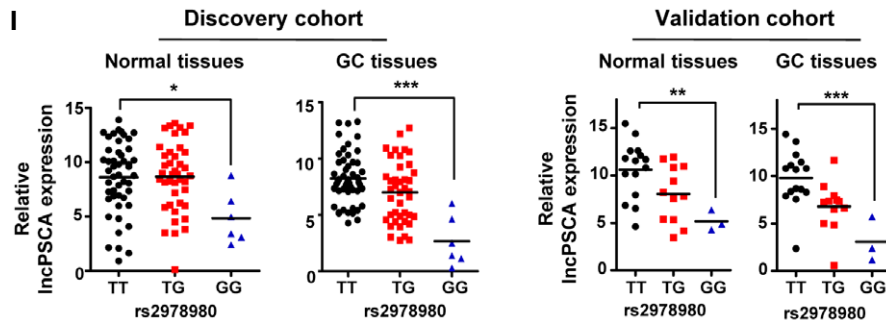
Figure 1.

oligonucleotides did not affect the binding activity of the T allele probe. Similar results were observed when using RORA-containing MGC80-3 nuclear extracts (Fig 1C). We also performed the EMSA competition assays using the RORA antibody (Appendix Fig S3). Interestingly, although the super-shift bands were not found, we did observe gradually attenuated RORA binding bands with increased amount of RORA antibody used for the rs2978980T probes in both GC cell lines (Appendix Fig S3A–C). Sanger sequencing indicated the MGC80-3 cell line carries the TG geno-type and HGC-27 has the GG genotype (Fig 1D). As a result, we further confirmed that the binding of RORA to the *lncPSCA* intronic enhancer region occurred *in vivo* in MGC80-3 cells using ChIP assays with *NPAS2* as the positive control. The *lncPSCA* enhancer region around rs2978980 SNP (region c), but not negative control regions (regions a and b), could be specifically precipitated with the RORA antibody (Fig 1E). Consistently, the positive control *NPAS2* promoter region (region d) could also be precipitated with the RORA antibody (Fig 1E). Silencing of *RORA* expression with siRNAs (siRORA mix) significantly reduced *lncPSCA* enhancer DNA or *NPAS2* promoter DNA precipitated compared to the NC RNA group (both $P < 0.01$; Fig 1E).

We further examined impacts of transcription factor RORA on *lncPSCA* expression. In MGC80-3 cells, suppression of *RORA* using siRNAs (siRORA-1 and siRORA-2) could markedly down-regulate *lncPSCA* expression ($P < 0.01$) (Fig 1F). However, silencing of *RORA* did not obviously change *lncPSCA* expression in HGC-27 cells with the rs2978980 GG genotype (Fig 1F). After detecting *RORA* and *lncPSCA* expression in GC tissues and adjacent normal tissues from patients of the discovery cohort ($n = 96$) and validation cohort ($n = 30$) (Appendix Table S2 and S3), we observed significantly positive expression correlations between *RORA* and *lncPSCA* in these specimens (both $P < 0.001$; Fig 1G). There was an evident lncPSCA down-regulation in GC tissues compared to normal tissues in discovery cohort or validation cohort (both $P < 0.05$; Fig 1H). Importantly, we found a significantly allele-differential lncPSCA expression between rs2978980G-allele carriers or T-allele carriers in either GC or normal tissues from both cohorts (all $P < 0.05$; Fig 1I), which is in support of the regulatory role of rs2978980 via differential binding of RORA.

Identification of *lncPSCA* as a novel GC-susceptibility gene

The CPAT tool (https://wlcb.oit.uci.edu/cpat/index.php) predicts that *lncPSCA* may have an open read frame (ORF) (Appendix Fig S4). To test this, we generated two GFP fusion protein constructs (pEGFP-N1-ORF and pEGFP-N1-5'UTR-ORF) as reported previously (Huang *et al*, 2017; Appendix Fig S4A). The pEGFP-N1-ORF construct includes the CPAT-predicted ORF (435–1,004 nt of NR_033343.2) and the pEGFP-N1-5'UTR-ORF construct includes the "so-called" 5'UTR (1–434 nt of NR_033343.2) plus ORF. These two constructs and pEGFP-N1 were transfected into HEK293T cells. After 48 h, obvious GFP was found in pEGFP-N1-transfected cells; however, expression of the fusion protein was not observed in pEGFP-N1-ORF or pEGFP-N1-5'UTR-ORF-transfected cells (Appendix Fig S4B). Similarly, the PhyloCSF prediction results indicated that lncPSCA does not have coding potential (Appendix Fig S4C). Taken together, these data revealed that *lncPSCA* does not encode a peptide.

Considering the role of *lncPSCA* in GC development is still unclear, we firstly studied whether silencing or overexpression of *lncPSCA* could modulate cell proliferation. Down-regulation of lncPSCA by siRNAs significantly accelerated proliferation of GC cells compared to cells transfected with NC RNA (all $P < 0.05$) (Appendix Fig S5A and B). On the contrary, elevated expression of lncPSCA significantly suppressed cell growth in different GC cells (all $P < 0.01$) (Appendix Fig S5C and D). To gain insight into the functional relevance of lncPSCA, we developed the CRISPR/Cas9-engineered *lncPSCA*-knockout GC cells (MGC80-3: KO-C1 and KO-C3; HGC-27: KO-C14 and KO-C40) (Fig 2A and B; Appendix Fig S6–S8) and the stably *lncPSCA*-overexpression GC cells (MGC80-3: lncP-C5 and lncP-C7; HGC-27: lncP-C1 and lncP-C10). As shown in Fig 2C, stable *lncPSCA*-knockout resulted in significantly enhanced proliferation of GC cell lines compared to the control cells ($P < 0.05$) (Fig 2C). Stable *lncPSCA* overexpression could obviously inhibit viability of GC cells ($P < 0.01$) (Fig 2C). Colony formation assays also supported the tumor suppressor role of *lncPSCA* in GC (Fig 2D and Appendix Fig S9). Considering that *PSCA* and *lncPSCA* share common exons and that both are tumor suppressor, we detected mRNA and protein expression levels of *PSCA* in the *lncPSCA*-knockout GC cells. We found that there were no evident *PSCA* expression changes in stable *lncPSCA*-knockout GC cells (Appendix Fig S10A and B).

We then evaluated the anticancer capability of lncPSCA *in vivo*. We found that the growth of the *lncPSCA*-knockout MGC80-3 or HGC-27 xenografts in mice was significantly accelerated compared with that of control xenografts after 27 or 18 days (Fig 2E). Evidently increased tumor weights were also observed in the *lncPSCA*-knockout group compared to the control group (Fig 2E). Ki67 protein levels in xenografts of the *lncPSCA*-knockout group were higher than those in control xenografts (Fig 2F).

Figure 2. lncPSCA suppresses gastric cancer cell proliferation *in vitro* and *in vivo*.

A   A diagram of sgRNA locations for development of the CRISPR/Cas9-engineered *lncPSCA*-knockout gastric cancer cells.

B   The detailed information of deleted sequences in various *lncPSCA*-knockout clones (MGC80-3: KO-C1 and KO-C3; HGC-27: KO-C14 and KO-C40).

C   In MGC80-3 and HGC-27 cells, *lncPSCA*-knockout resulted in significantly enhanced cell proliferation comparing with the control cells. Stably *lncPSCA* overexpression could obviously inhibit viability of gastric cancer cells. Data show one representative example of three biological replicates.

D   Colony formation assays. Upper subpanel: photos of cell clones in each well; lower subpanel: numbers of cell clones in each well. Data show one representative example of three biological replicates.

E   *lncPSCA*-knockout significantly promoted growth of MGC80-3 ($n = 8$) or HGC-27 ($n = 7$) xenografts compared with control xenografts after 27 or 18 days.

F   HE and Ki67 staining of MGC80-3 or HGC-27 xenografts. Scale bar = 100 μm.

Data information: Each value represents mean ± SD. The difference between two groups was calculated using Student's *t* test. *$P < 0.05$; **$P < 0.01$, ***$P < 0.001$.

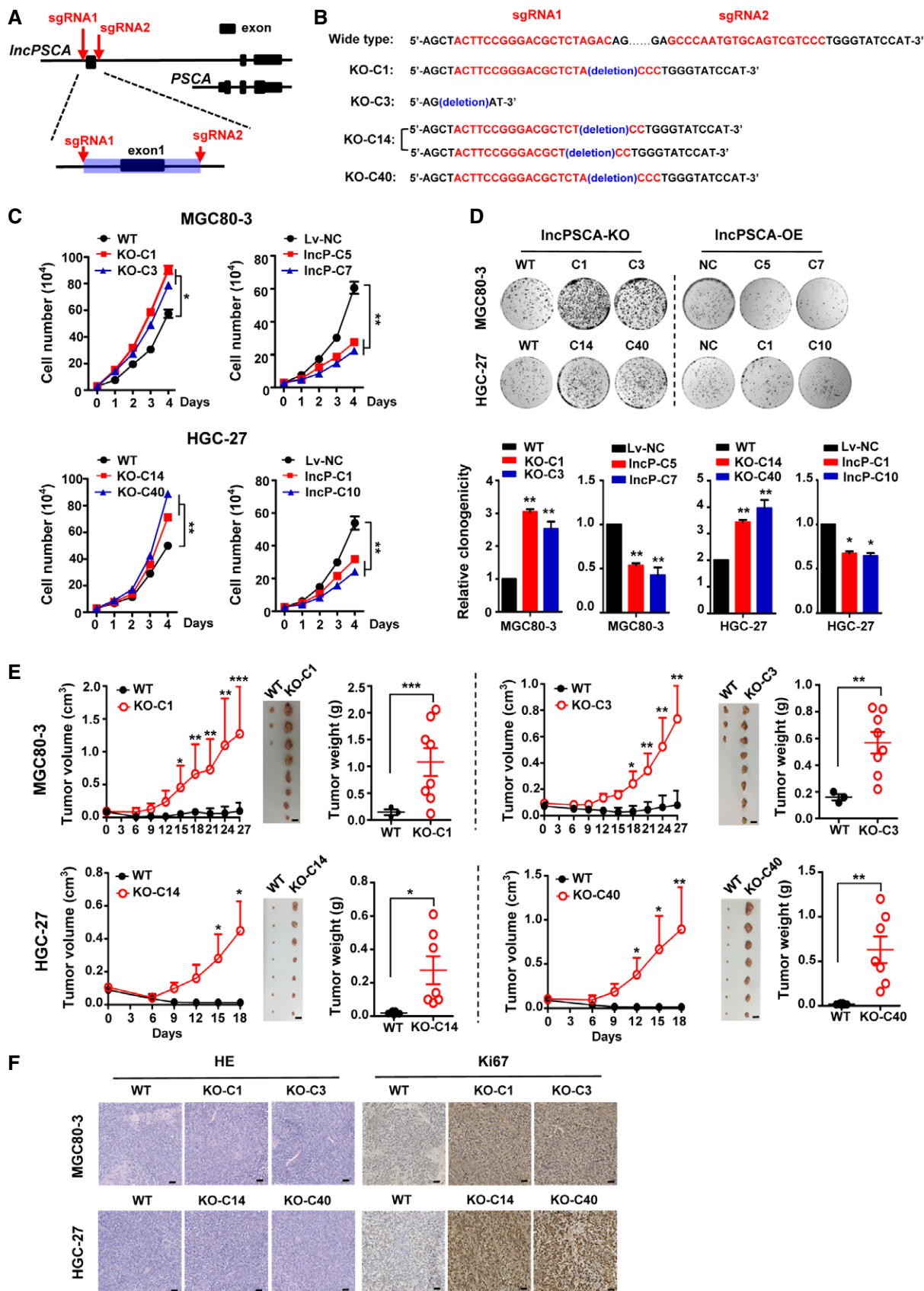**Figure 2.**

LncPSCA inhibits GC invasion and metastasis *in vitro* and *in vivo*

We next examined whether *lncPSCA* could influence migration, invasion and metastasis of GC cells. The wound-healing assays demonstrated that *lncPSCA* knockdown with siRNAs or stable *lncPSCA* knockout with the CRISPR/Cas9 system promoted migration of MGC80-3 and HGC-27 cells (Appendix Fig S11A–C and S12A–D; Fig 3A). In contrast, overexpression of *lncPSCA* impaired cell motility (Appendix Fig S11A–C and S12A–D; Fig 3A). The impact of *lncPSCA* on invasiveness of MGC80-3 and HGC-27 cells was determined using the Matrigel invasion assays. Silencing or knockout of *lncPSCA* can enhance invasion of MGC80-3 and HGC-27 cells (Appendix Fig S11A–C and S12A–D; Fig 3B). In line with this observation, reduced invasion capability of GC cells was observed after elevated *lncPSCA* expression (Appendix Fig S11A–C and S12A–D; Fig 3B). To investigate the mechanistic rationale, we measured the expression of four markers of epithelial-to-mesenchymal transition (EMT) in GC cells. Intriguingly, lncPSCA could significantly promote expression of β-catenin and ZO-1 and inhibit expression of SNAIL and VIMENTIN. Knockout of *lncPSCA* reduced β-catenin and ZO-1 expression and stimulated expression of SNAIL and VIMENTIN (Fig 3C and Appendix Fig S13A–C). These results suggested that lncPSCA may inhibit EMT of GC cells and result in decreased cell migration and invasion.

We then explored the biological significance of *lncPSCA* during *in vivo* metastasis of GC cells. The tail vein injection mouse model further proved that knockout of *lncPSCA* can remarkably accelerate lung metastasis and brain metastasis of GC cells (Fig 3D). These results were confirmed by histological analyses of the metastasis tumors (Fig 3E). Incidence of distant metastases in nude mice was showed in Fig 3F. Collectively, these findings indicated that *lncPSCA* suppresses GC metastasis *in vitro* and *in vivo*.

LncPSCA promotes DDX5 degradation

Since lncRNAs could function through interacting with various proteins, we speculated that lncPSCA may interact with certain protein(s) to impact GC development. To test this hypothesis, we firstly examined cellular localization of lncPSCA and found that it is predominantly in the nuclear fraction of GC cells (Fig 4A). Using RNA pull-down assays with HGC-27 nucleus extracts, we observed multiple proteins which could be pulled-down by lncPSCA (Fig 4B). Mass spectrometry proteomics indicated that the most abundant protein among these proteins was DDX5 (Appendix Table S4). We then validated seven candidate proteins through independent RNA pull-down assays and successfully verified DDX5 (Fig 4C). RNA immunoprecipitation (RIP) assays also confirmed more than 100-fold enrichment of lncPSCA in RNA-protein complexes precipitated with antibody against DDX5 as compared with the IgG control in GC cells (P < 0.001) (Fig 4D). During RIP, *HOTTIP* was used as the negative control and *SRA* as the positive control (Fig 4D).

We then examined the molecular consequences of the interaction between lncPSCA and DDX5. Although the expression levels of *DDX5* mRNA were not changed (Appendix Fig S14A–E), the expression levels of DDX5 protein were markedly suppressed when lncPSCA was overexpressed (Fig 4E and Appendix Fig S14A–E). Treatment of the *lncPSCA*-knockout GC cells with the protein synthesis inhibitor CHX increased expression of endogenous DDX5 protein compared to wild-type GC cells (Fig 4F and Appendix Fig S14A–E). Conversely, treatment of GC cells overexpressing *lncPSCA* with CHX resulted in a notably shorter half-life of DDX5 protein than in control cells (Fig 4F and Appendix Fig S14A–E), suggesting that lncPSCA may be involved in regulating degradation of DDX5 protein through the ubiquitin-proteasome pathway. As expected, the ubiquitination of DDX5 was strikingly increased in cells overexpressing lncPSCA in comparison with control cells (Fig 4G). After exogenous DDX5 was immunoprecipitated in HEK293T cells transfected with HA-ubi and FLAG-DDX5, evidently increased ubiquitin signals of DDX5 protein were found in cells after lncPSCA overexpression (Fig 4G). Consistent with this, obviously elevated ubiquitin signals of endogenous DDX5 protein were detected in HGC-27 cells overexpressing lncPSCA compared to the control GC cells (Fig 4G). Taken together, these data elucidated that lncPSCA accelerates degradation of DDX5 through ubiquitination. Consistent to the TCGA STAD data, evidently increased *DDX5* expression was found in our GC patient cohorts (all P < 0.05) (Fig 4H). Silencing of *DDX5* expression with siRNAs or shRNA impaired viability and clonogenic capacity of GC cells (Fig 4I–K; Appendix Fig S15A–C), suggesting a strong oncogenic potential of *DDX5* in GC.

Silencing DDX5 activates the Pol II-controlled gene transcription program

DDX5 is a multifunctional RNA binding protein and RNA Pol II has been identified as a DDX5 partner in nucleus of prostate cancer cells (Clark *et al*, 2013; Nyamao *et al*, 2019). Considering the importance of RNA Pol II in controlling the gene transcription program, we firstly examined whether DDX5 is also a partner protein of RNA Pol II in GC cells. Co-IP assays showed that endogenous RNA Pol II precipitated with DDX5 and, in contrast, endogenous DDX5 also precipitated with RNA Pol II in GC cells under physiological conditions (Fig 5A). As a result, we performed ChIP-seq of total RNA Pol II to investigate impacts of DDX5 on the genome-wide gene transcription program in HGC-27 cells after silencing of *DDX5* (lv-shD). We plotted the normalized tag counts from the RNA Pol II ChIP-seq data. Intriguingly, when normalized to the same sequencing depth, the RNA Pol II signals were much stronger in GC cells with silenced *DDX5* expression compared to those in negative control cells (lv-NC) (Fig 5B). We observed prominently enriched RNA Pol II signals along the genome and increased RNA Pol II enrichment in HGC-27 cells after silencing of *DDX5* compared to the control group (Fig 5C). Together, the results indicated that that silencing of *DDX5* dramatically enhances RNA Pol II enrichment along human chromatin in GC.

Next, we identified significantly differential expressed genes (DEGs) in HGC-27 cells after overexpression of *lncPSCA* or silencing of *DDX5* (Fig 5D). There were 863 significantly up-regulated genes and 217 down-regulated genes after overexpression of *lncPSCA* (Fold change > 1.5, P < 0.05). Silencing of *DDX5* resulted in 894 significantly up-regulated genes and 452 down-regulated genes. A total of 168 overlapped DEGs were identified in cells after overexpression of *lncPSCA* or silencing of *DDX5*. KEGG pathway analyses of these overlapped DEGs revealed that they were enriched for multiple pathways involved in cancer
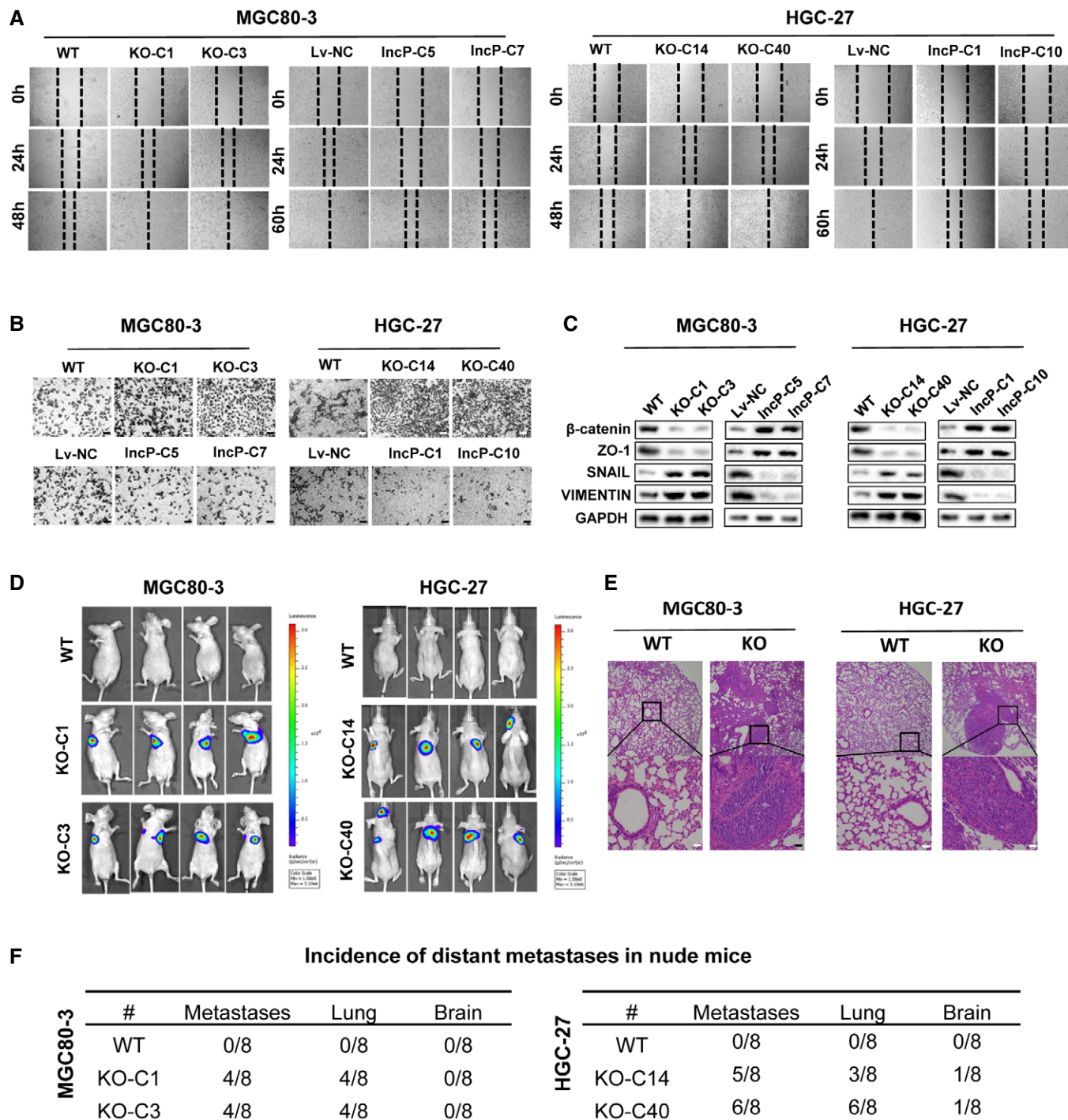
A

B

C

D

E

F

Incidence of distant metastases in nude mice

MGC80-3	#	Metastases	Lung	Brain
	WT	0/8	0/8	0/8
	KO-C1	4/8	4/8	0/8
	KO-C3	4/8	4/8	0/8

HGC-27	#	Metastases	Lung	Brain
	WT	0/8	0/8	0/8
	KO-C14	5/8	3/8	1/8
	KO-C40	6/8	6/8	1/8

Figure 3. lncPSCA reduces migration, invasion, and metastasis capabilities of gastric cancer cells.

A   In MGC80-3 and HGC-27 cells, *lncPSCA*-knockout accelerates wound-healing and the stably enforced lncPSCA expression inhibits wound-healing. The dashed lines indicate the edges of the cell layers.

B   lncPSCA inhibits invasion abilities of MGC80-3 and HGC-27 cells. Cells on the lower surface of the chamber were stained by crystal violet. Scale bar = 100 μm.

C   In MGC80-3 and HGC-27 cells, expression changes of different markers (β-catenin, ZO-1, SNAIL, and VIMENTIN) of epithelial-to-mesenchymal transition were examined after overexpression or knockout of *lncPSCA*.

D   Fluorescent images of tumors in nude mice with tail vein injected MGC80-3 and HGC-27 cells with or without knockout of *lncPSCA*.

E   Representative images of hematoxylin and eosin-stained slides of lung metastatic nodules of MGC80-3 and HGC-27 with or without knockout of *lncPSCA*. Scale bar = 100 μm.

F   Incidence of distant metastases in nude mice (*n* = 8 per group).

Source data are available online for this figure.

biology, with the P53 and MAPK signaling pathways as two of the most markedly changed pathways (Fig 5D). To further explore impacts of altered lncPSCA levels on the P53 or MAPK signaling, we plotted the histogram of RNA Poll II ChIP-seq and RNA-seq read counts for four P53 signaling candidate genes (*PMAIP1, CDKN1A, SESN2,* and *SESN3*) (Fig 5E) and nine MAPK signaling candidate genes (*JUN, VEGEA, FGF21, ANGPTL1,*

NGFR, RASGRP3, MAPT, HSPA8, and *HSPA1B*) (Appendix Fig S16). Notably, *PMAIP1, CDKN1A,* and *SESN2* showed increased RNA Poll II enrichment around gene TSS as well as elevated RNA-seq signals in GC cells when lncPSCA was overexpressed or *DDX5* expression was silenced (Fig 5E). However, no such consistent ChIP-seq and RNA-seq results were observed for the MAPK signaling candidate genes (Appendix Fig S16). To verify
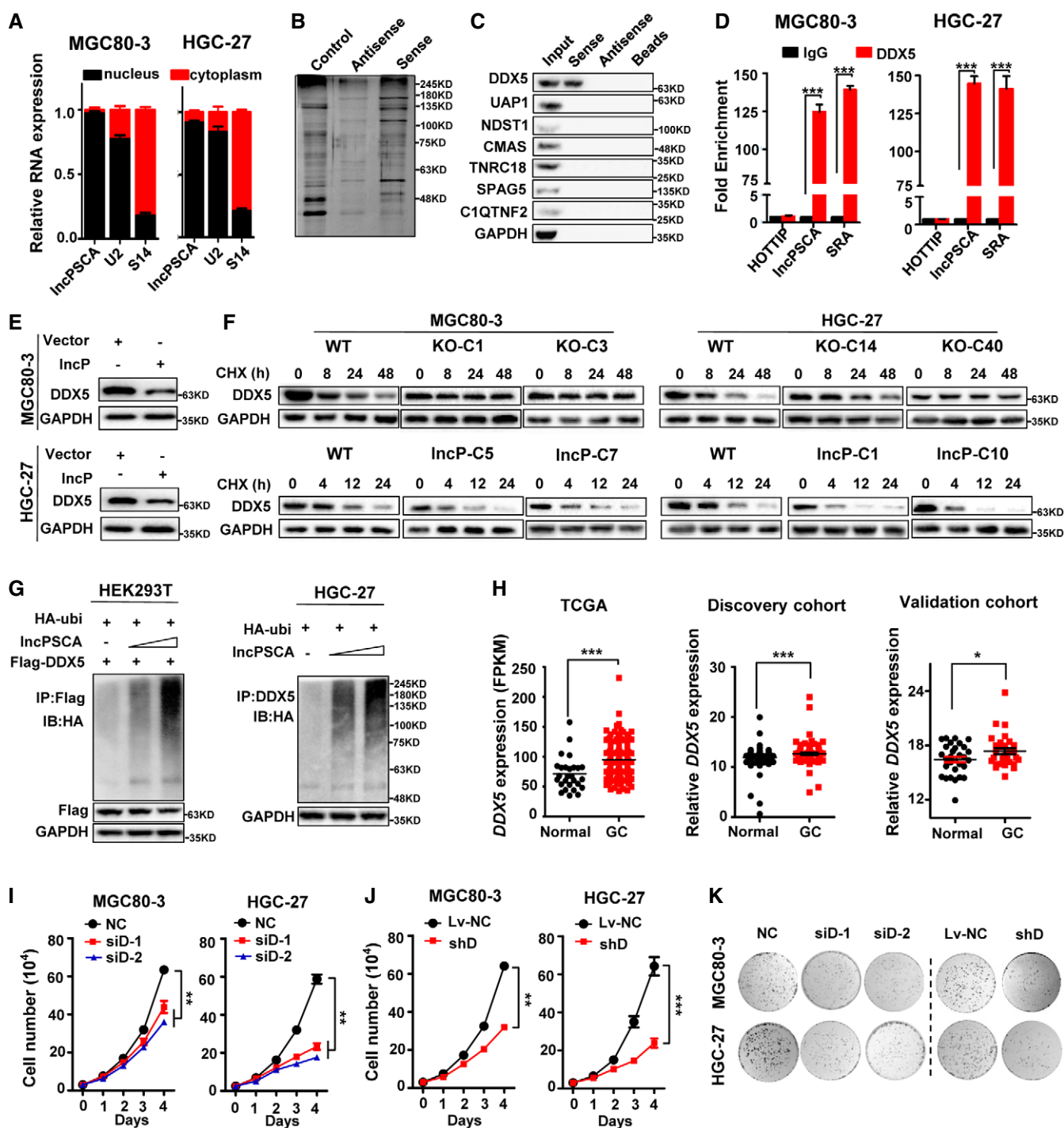

Figure 4.

◄

Figure 4. lncPSCA interacts with DDX5 and promotes DDX5 degradation.

A   lncPSCA predominantly locates in the nuclear fraction of gastric cancer cells. In detail, the cytosolic and nuclear fractions of HGC-27 or MGC80-3 cells were separately isolated. RNA was isolated from either the cytosolic fraction or the nuclear fraction. Expression of lncPSCA in the cytosolic and nuclear RNA was measured. Data show one representative example of three biological replicates.

B   Silver staining of lncPSCA pull-down nuclear proteins of gastric cancer cells.

C   lncPSCA pull-down followed by Western blot validated its interaction with DDX5 and other candidate proteins identified by mass spectrometry. GAPDH served as the control.

D   RIP assays show association of DDX5 with lncPSCA in MGC80-3 and HGC-27 cells. Relative enrichment (means ± SD) represents RNA levels associated with DDX5 relative to an input control from three independent experiments. IgG served as the control. *HOTTIP* was used as the negative control and *SRA* as the positive control during RIP. Data show one representative example of three biological replicates.

E   Western blot analyses of DDX5 protein in gastric cancer cells with the enforced expression of *lncPSCA*.

F   Gastric cancer cells after *lncPSCA*-knockout or stably overexpressing *lncPSCA* and control cells were treated with cycloheximide (CHX) or vehicle for the indicated periods of time. DDX5 levels were analyzed by Western blot.

G   Western blot to detect the ubiquitination of DDX5 in HEK293T cells cotransfected with pcDNA-lncPSCA, HA-Ubiquitin and Flag-DDX5 (left panel) or in HGC-27 cells cotransfected with pcDNA-lncPSCA and HA-Ubiquitin (right panel).

H   Expression of *DDX5* was compared between normal and gastric cancer samples in TCGA cohort (left), Shandong discovery cohort (middle) and Shandong validation cohort (right).

I   Knockdown of *DDX5* with siRNA (siD-1 and siD-2) substantially reduced the proliferation of gastric cancer cells. Data show one representative example of three biological replicates.

J   Silencing of *DDX5* with shRNA (shD) significantly reduced the proliferation of gastric cancer cells. Data show one representative example of three biological replicates.

K   Effects of *DDX5* knockdown on the colony formation of gastric cancer cells. HGC-27 or MGC80-3 were seeded into a 6-well cell culture plate and transfected with *DDX5* siRNAs (siD-1 and siD-2). The HGC-27 or MGC80-3 cells stably transfected with the *DDX5* shRNA (shD) were seeded into a 6-well culture plate. When colonies were visible after 14 days, cells were washed with cold PBS twice and fixed with the fixation fluid. Cells were stained with crystal violet, and photographs were taken.

Data information: The difference between two groups was calculated using Student's *t* test. *$P < 0.05$, **$P < 0.01$, ***$P < 0.001$.
Source data are available online for this figure.

the ChIP-seq and RNA-seq data, we examined mRNA levels and RNA Poll II enrichment of *PMAIP1, CDKN1A* and *SESN2* in stable *lncPSCA*-overexpression, *lncPSCA*-knockout and *DDX5*-knockdown cells via RT-qPCR and ChIP-qPCR (Fig 5F and G). In line with the RNA-seq data, *lncPSCA*-overexpression and *DDX5*-knockdown evidently up-regulated expression of these genes; whereas, *lncPSCA*-knockout suppressed mRNA levels of the genes. Consistent to the ChIP-seq data, ChIP-qPCR assays demonstrated that significantly decreased RNA Poll II enrichment around TSS of *PMAIP1, CDKN1A,* and *SESN2* in stable *lncPSCA*-knockout GC cells. In support of these, the expression levels of *PMAIP1, CDKN1A,* and *SESN2* was significantly down-regulated in the GC samples compared to normal tissues in discovery cohort and validation cohort (Appendix Fig S17A), supporting their tumor suppressor nature. Importantly, we observed significantly positive expression correlations between lncPSCA and *PMAIP1, CDKN1A,* or *SESN2* in either GC tissues or normal gastric tissues in both cohorts (Fig 5H and Appendix Fig S17B). Collectively, these results suggested that lncPSCA-mediated DDX5 degradation activates the RNA Poll II-controlled transcription program of multiple tumor suppressor genes.

Discussion

The chromosome 8q24.3 is the first GWAS-reported GC-susceptibility locus in Japanese populations and this association has been replicated in populations of different ethnicities, including Chinese (Abnet *et al*, 2010; Shi *et al*, 2011; Wang *et al*, 2017; Zhu *et al*, 2017), Korean (Wang *et al*, 2017), American (Wang *et al*, 2017; Zhu *et al*, 2017), and European (Helgason *et al*, 2015) populations. Protein-coding *PSCA* gene was previously considered as the GC-susceptibility gene accounting for the lead variant rs2294008

(Sakamoto *et al*, 2008; Saeki *et al*, 2015; Sung *et al*, 2016). However, the biological mechanisms of the noncoding transcript of *PSCA* (*lncPSCA*) at 8q24.3 in GC development have not been investigated. In the present study, we found that the protective T allele of GC risk SNP rs2978980 may promote activities of a *lncPSCA* intronic enhancer by binding transcriptional factor RORA and increase the tumor suppressive lncRNA expression. Additionally, significantly lower lncPSCA levels have been found in GC specimens as compared with normal tissues. We also demonstrated that lncPSCA can interact with DDX5 and facilitate ubiquitination and degradation of DDX5. Increased expression of lncPSCA in cells resulted in low levels of DDX5, less RNA Pol II binding with DDX5, and, thus, activated transcription of multiple P53 signaling tumor suppressors by Pol II. These results provide new evidences for our understanding on the genetic basis of GC risk and highlight importance of lncRNA-mediated controlling of transcription programs involved in tumorigenesis (Fig 6).

In recent years, tens of thousands of lncRNAs have been found in human via high-throughput sequencing technologies. Accumulated amount of evidences has expanded our perception of lncRNAs from "transcriptional junk" to functional biological molecules regulating cellular processes including post-transcriptional modifications, transcription, chromatin remodeling, and signal transduction (Leucci, 2018; Statello *et al*, 2021). In GC, several lncRNAs have been shown to be differentially expressed in cancerous tissues and are implicated in malignant transformation and metastasis (Liu *et al*, 2018; Zhang *et al*, 2018a,b,c; He *et al*, 2019; Sakai *et al*, 2019; Wang *et al*, 2019; Xu *et al*, 2019; Zhuo *et al*, 2019). However, the regulation of expression and functions of most lncRNAs in GC remains to be elucidated. Genetic variations in lncRNA gene enhancer sequences have the potential to create novel binding motifs of transcription factor(s) that may be selected in cancer cells (Pan *et al*, 2016; Gao *et al*, 2018; Hua *et al*, 2018). One such
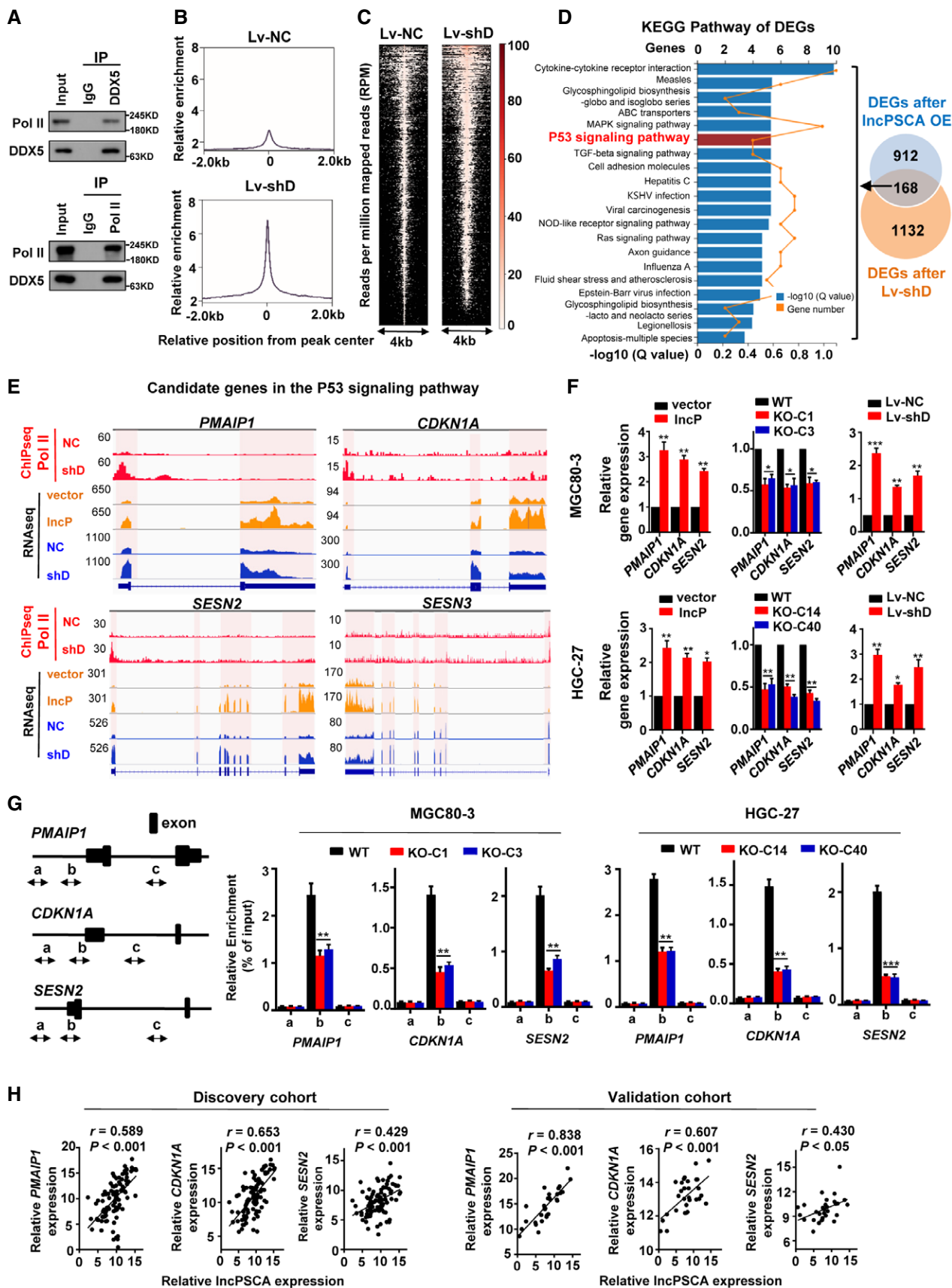
Figure 5.

Figure 5. lncPSCA-induced degradation of DDX5 releases RNA Pol II from the DDX5-Pol II complex in nucleus.

A   Western blot for RNA Pol II among proteins pulled down with anti-DDX5 (up) and for DDX5 among proteins pulled down with an anti-Pol II antibody (down).
B   Global increase in RNA Pol II signals after silencing of *DDX5* (lv-shD) in HGC-27 cells. Average RNA Pol II ChIP-seq signal at all RNA Pol II peak regions. Upper subpanel: negative control, Lv-NC; lower subpanel: silencing of *DDX5*, lv-shD.
C   Reads per million mapped reads (RPM) of RNA Pol II ChIP-seq signals of genes in human genome.
D   KEGG Pathway analyses of overlapped differential expressed genes (DEGs) in both lncPSCA-overexpression cells and the *DDX5*-konckdown cells identified multiple pathways involved in cancer biology, with the P53 and MAPK signaling pathways as two of the most markedly changed pathways.
E   RNA Pol II ChIP-seq and RNA-seq signals of *PMAIP1*, *CDKN1A*, *SESN2*, and *SESN3* in HGC-27 cells. Red bars represent the RNA Pol II ChIP-seq signal. Orange or blue bars represent the RNA-seq signals of HGC-27 cells overexpressing *lncPSCA* (lncP) or with silenced *DDX5* (shD), respectively.
F   Validation of candidate downstream genes of the lncPSCA-DDX5 axis identified through the integrated analyses. RT–qPCR was performed for *PMAIP1*, *CDKN1A*, and *SESN2* genes upon overexpression of *lncPSCA* (lncP), silencing of *DDX5* (shD) or *lncPSCA* knockout. Error bars indicate the SEM. Data show one representative example of three biological replicates.
G   ChIP-qPCR assays were performed for *PMAIP1*, *CDKN1A*, and *SESN2* genes and demonstrated that significantly decreased RNA Poll II enrichment around TSS of *PMAIP1*, *CDKN1A* and *SESN2* in various stable *lncPSCA* knockout GC cell lines. Left subpanel: RNA Pol II ChIP-qPCR fragments a, b, and c on *PMAIP1*, *CDKN1A*, and *SESN2* genes; middle and right subpanels: RNA Pol II ChIP-qPCR results of *PMAIP1*, *CDKN1A*, and *SESN2* genes in MGC80-3 (middle) and HGC-27 cells (right). Data show one representative example of three biological replicates.
H   Correlations between lncPSCA levels and the mRNA levels of the P53 signaling *PMAIP1*, *CDKN1A*, and *SESN2* genes in gastric cancer tissues discovery cohort ($n = 96$) and validation cohort ($n = 30$). RNA levels were determined by RT–qPCR relative to *GAPDH*. The *r* values and *P* values are from Pearson's correlation analyses.

Data information: The difference between two groups was calculated using Student's *t* test. The significance of expression association between different genes was calculated using Spearman's correlation. *$P < 0.05$, **$P < 0.01$, ***$P < 0.001$.
Source data are available online for this figure.

example is a prostate cancer risk-associated SNP rs11672691 and its LD SNP rs887391, which decrease binding of transcription factors NKX3.1 and YY1 to the promoter of lncRNA *PCAT19*-short, resulting in weaker promoter but stronger enhancer activity that subsequently activates oncogenic lncRNA *PCAT19*-long (Hua *et al*, 2018). Our study, for the first time, demonstrated that GC risk SNP rs2978980 T > G could down-regulate *lncPSCA* expression via interrupting RORA binding to its enhancer and increase cancer susceptibility. Our results, along with findings in previous reports (Guo *et al*, 2016; Betts *et al*, 2017; Cho *et al*, 2018; Gao *et al*, 2018; Hua *et al*, 2018; Leucci, 2018; Moradi Marjaneh *et al*, 2020; Statello *et al*, 2021), highlight the understanding of functional impotence of the regulatory mechanisms of lncRNAs transcribed from GWAS-identified risk loci during tumorigenesis and progression.

In this study, we also demonstrated that lncPSCA can interact with DDX5 protein and promote proteasome-mediated degradation of DDX5. Human RNA helicase DDX5 is a member of a highly conserved protein family involved in gene expression regulation (Nyamao *et al*, 2019). DDX5 shows profound implications for cancer development and has been reported to be aberrantly expressed in many tumors (Nyamao *et al*, 2019). In line with this, we found that DDX5 exhibited oncogenic activity and was significantly up-regulated in GC tissues. Our study showed that DDX5 is a partner of RNA Pol II in nucleus of GC cells. DDX5 degradation caused by elevated lncPSCA expression resulted in more Pol II released from the DDX5-Pol II complex and promoted transcription of P53 signaling genes, which thereby inhibiting tumor growth and metastasis.

The P53 signaling serves as one of the most crucial tumor suppressive pathways in the development and progression of multiple malignancies (Kruiswijk *et al*, 2015; Cheok & Lane, 2017). We found that, in GC cells, up-regulated lncPSCA decreased DDX5 levels, which thus may potentially have promoted RNA Pol II-controlled stimulation of the P53 signaling, leading to elevated *PMAIP1*, *CDKN1A*, and *SESN2* expression and subsequently suppressed proliferation of GC cells. Moreover, we observed positive correlations between lncPSCA levels and the mRNA levels of *PMAIP1*, *CDKN1A*, and *SESN2* in both GC and normal tissues. These results suggested the activation effect of lncPSCA on the P53 signaling via DDX5. *PMAIP1*, also known as *NOXA*, is a primary P53-response gene and appears to be crucial in fine-tuning cell death decisions by targeting the pro-survival protein MCL1 for proteasomal degradation (Ploner *et al*, 2008). As one of BCL2 homology domain 3 (BH3)-only proteins, activation of PMAIP1 appears critical for the cellular response to anticancer treatment regimens, such as γ-irradiation and chemotherapeutic drugs (i.e., Venetoclax/ABT-199) (Ploner *et al*, 2008). *CDKN1A* (*P21/WAF1*), is a universal cell-cycle inhibitor directly controlled by P53 and acting to restrain tumor proliferation (El-Deiry, 2016). Another important molecule downstream of the lncPSCA-DDX5 axis is *SESN2* which is an antioxidant gene activated by P53. SESN2 is critical for suppression of reactive oxygen species and protection from oxidative stress, transformation, and genomic instability in a P53-dependent manner. *SESN2* knockout cells are more susceptible to Ras+E1A-induced transformation than their wild-type counterparts (Budanov, 2011). Because *PMAIP1*, *CDKN1A*, and *SESN2* are all critical P53-dependent tumor suppressors, decreased levels of these genes by lncPSCA may contribute to cell transformation and tumorigenesis.

In summary, by fine-mapping the 8q24.3 GC risk locus and functional characterization, we have identified a lncRNA, *lncPSCA*, as a novel susceptibility gene that acts through regulation of DDX5 stability and RNA Pol II-controlled transcriptional programs, leading to inhibited proliferation and metastasis of cancer cells. The enhancer rs2978980 T > G genetic variant impairs expression and anti-neoplasm effect of lncPSCA and confers susceptibility to GC. These findings shed new light on the importance of functionally annotating lncRNAs in GWAS risk loci and further declaration of aberrantly expressed lncRNA in the etiology of human malignancies. Given that the majority of lncRNAs display remarkable cell and tissue-specific expression, understanding the function of these lncRNAs therefore holds great potential for innovative cancer therapies.

Gastric cancer susceptibility 8q24 locus
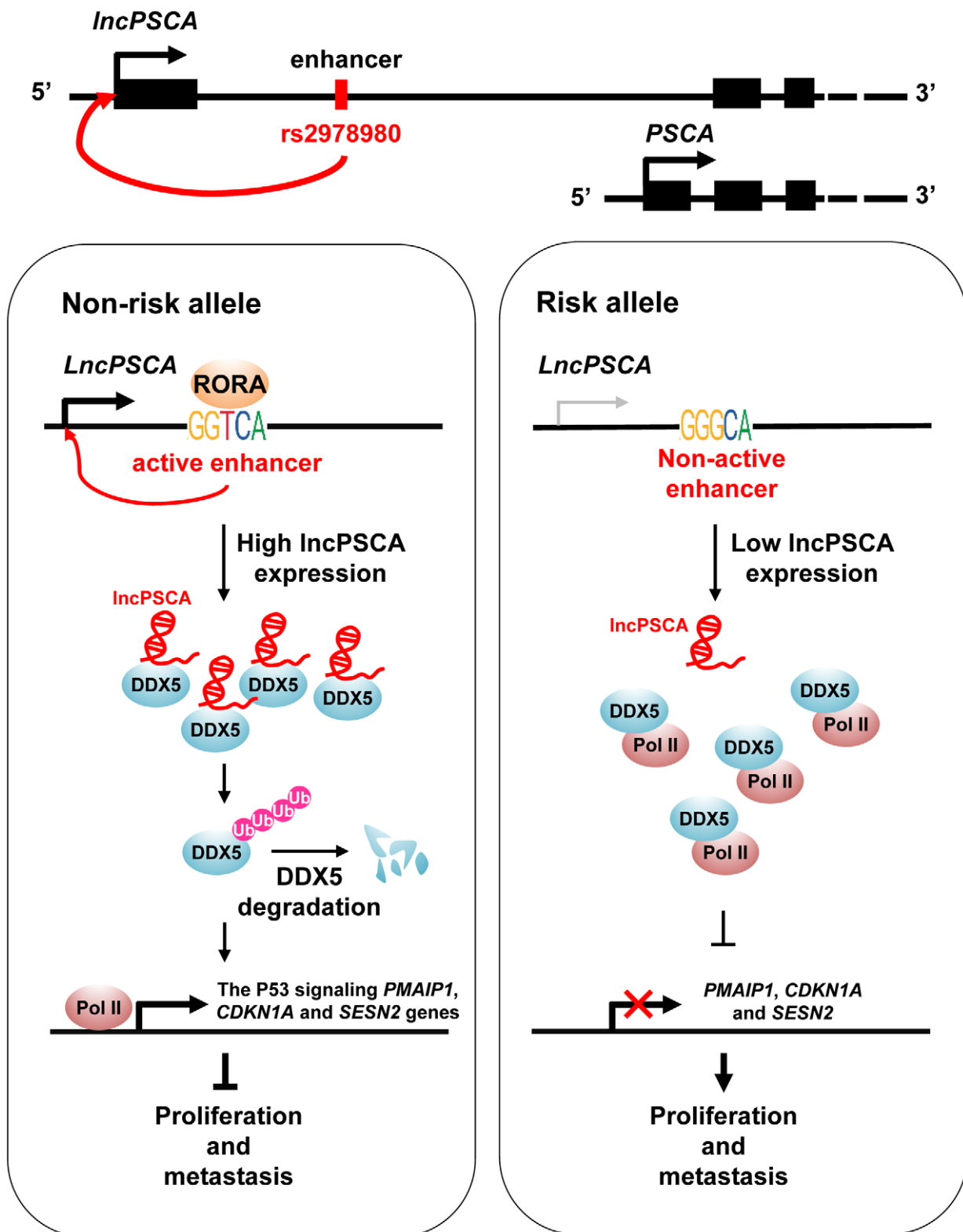
Figure 6. Graphical representation of the regulation and function of *lncPSCA* in gastric cancer.

The gastric cancer risk-associated rs2978980 T > G genetic variant disrupts RORA binding to the intronic enhancer region of *lncPSCA* and down-regulates lncPSCA expression in cells. LncPSCA is a tumor suppressive lncRNA that acts by controlling DDX5 degradation through ubiquitination, resulting in released RNA Pol II from the DDX5-Pol II complex and activated transcription and expression of the P53 signaling genes that are important for gastric cancer progression.

Materials and Methods

Cell culture

Human GC HGC-27 cells were cultured in RPMI 1640 medium (Gibco, C11875500BT). Human MGC80-3 and HEK293T cells were cultured in DMEM medium (Gibco, C11995500BT). All media were supplemented with 10% fetal bovine serum (FBS; Gibco, 1347575). Cells were maintained at 37°C in a 5% CO_2 incubator and periodically tested mycoplasma negative.

Electrophoretic mobility-shift assays

Synthetic double-stranded and 3' biotin-labeled DNA oligonucleotides corresponding to the RORA consensus binding sequence, rs2978980T or rs2978980G sequences were synthesized by Thermo Fisher (Beijing, China) (Appendix Table S5). HGC-27 or MGC80-3 cell nuclear extracts and these DNA oligonucleotides were incubated at 25°C for 20 min using the Light Shift Chemiluminescent EMSA Kit (Pierce, 20148). The reaction mixture was separated on 6% PAGE and detected by Stabilized Streptavidin-Horseradish Peroxidase Conjugate (Pierce, SA10001). In competition assays, unlabeled DNA probes at 100-fold molar excess were added to the reaction mixture before the addition of biotin-labeled oligonucleotides.

Cell transfection

Small interfering RNA (siRNA) duplexes for lncPSCA, *RORA,* or *DDX5* were products of Genepharma (Shanghai, China) (Appendix Table S5). The negative control RNA duplex (NC) for siRNAs (Genepharma) was nonhomologous to any human genome sequence. All small RNAs were transfected with the INTERFERin reagent (Polyplus, 409-10) as reported previously (Zhang *et al*, 2020). All plasmids were transfected with the jetPRIME reagent (Polyplus, 114-07) or Lipofectamine 2000 (Thermo Fisher, 11668019).

Quantitative reverse transcription PCR (RT–qPCR)

Total RNA was isolated from culture cells or tissue specimens with TRIzol reagent (Invitrogen, 94402). To remove genomic DNA, each RNA sample was treated with DNase I (RNase-free) (Thermo Fisher, 18068015). Each RNA sample was then reverse transcribed into cDNAs using PrimeScript™ RT Master Mix (TaKaRa, RR036A). The relative expression of lncPSCA, *RORA, DDX5, CDKNIA, PMAIP1,* and *SESN2* were calculated by using the $2^{-\Delta\Delta Ct}$ method. Indicated primers are listed in Appendix Table S5. Each sample was examined at least in triplicate. PCR product specificity was confirmed by a melting-curve analysis.

Western blot

Western blot was performed following the standard protocol as previously reported (Zhang *et al*, 2020). In brief, total cellular proteins were separated with SDS–PAGE gel and transferred to a polyvinylidene fluoride (PVDF) membrane (Millipore, ISEQ00010). The PVDF membrane was then incubated with various antibodies (Appendix Table S6) overnight at 4°C. Target proteins were visualized with ECL Western Blotting Substrate (Pierce, 32106).

Chromatin Immunoprecipitation Sequencing (ChIP-seq) and ChIP-qPCR

For ChIP assays, 2.5×10^7 HGC-27 or MGC80-3 cells were cross-linked using 1% formaldehyde for 10 min at 25°C. Reactions were quenched by addition of 250 mmol/l glycine for 5 min. Cells were lysed with the cell lysis/wash buffer (150 mmol/l NaCl, 5 mmol/l EDTA [pH7.5], 50 mmol/l Tris–HCl [pH7.5], 0.5% NP-40) plus protease inhibitor for 10 min on ice. Each sample was solved in the shearing buffer (1% SDS, 10 mmol/l EDTA [pH8.0], 50 mmol/l Tris–HCl [pH8.0]) plus protease inhibitor. Chromatin fragmentation was performed using a Diagenode BioruptorPlus sonicator (30 s on and 30 s off for 12 cycles) to achieve a DNA shear length of 200–500 bp. Solubilized chromatin was incubated with 15 μg anti-RORA antibody (Abcam, ab60134), anti-Pol II antibody (Millipore, 05-623), or IgG control (Invitrogen, 02-6102) (Appendix Table S6) overnight at 4°C on a rotating wheel. Antibody-chromatin complexes were subsequently pulled-down by incubating with Dynabeads® Protein G beads at 4°C for 4 h on a rotating wheel. Immune complexes were then washed for six times with the cell lysis/wash buffer at 4°C and then washed twice with the cold TE buffer (Invitrogen, 12090015). Elution and reverse-crosslinking were performed in the elution buffer (100 mmol/l $NaHCO_3$ and 1% SDS) on a shaker at 25°C for 15 min. After repeating the elution with the elution buffer, antibody-bound chromatin complexes were reversed cross-linked at 65°C with 5 mol/l NaCl overnight. After reversal of crosslink, each sample was treated with 50 ng/μl RNase A at 37°C for 30 min and, then, 10 mmol/l Proteinase K at 45°C for 1 h. Immunoprecipitated DNA was extracted with the Min-Elute PCR purification kit (Qiagen, 28004), followed by DNA library preparation and sequencing on the BGISEQ-500 platform (BGI, Shenzhen, China). For ChIP-qPCR assays, the fold enrichment of purified ChIP DNA relative to input DNA at a given genomic site was determined using TB Green® Premix Ex Taq™ I (Tli RNaseH Plus) (TaKaRa, RR820A). As previously described (Pan *et al*, 2018), ChIP-qPCR reactions were conducted with ChIP-qPCR primers in Appendix Table S5.

Patients and tissue specimens

There were two GC cohorts, discovery cohort ($n = 96$) and validation cohort ($n = 30$) recruited in the current study. All patients received curative surgical resection for GC in Shandong Cancer Hospital and Institute between August 2012 and October 2019 (discovery cohort) or between November 2019 and December 2020 (validation cohort). Prior to the surgery, no patients received any local or systemic anticancer treatments. Fresh GC specimens and matched adjacent normal stomach tissues were obtained from these patients. The normal tissues were sampled at least 2 cm away from the margin of the tumor. All subjects were ethnic Han Chinese. The detailed characteristics of all GC patients were shown in Appendix Table S2 and S3. This study was approved by the Institutional Review Board of Shandong Cancer Hospital and Institute. At recruitment, written informed consent was obtained from each subject. The methods were carried out in accordance with the approved guidelines.

LncPSCA expression constructs

The full-length *lncPSCA* cDNA (NR_033343.1) was directly synthesized by Genewiz (Suzhou, Jiangsu) and cloned after the CMV promoter of the pcDNA3.1 vector. The plasmid was named as pcDNA-lncPSCA. The full-length *lncPSCA* cDNA was also cloned into the pLVX-Puro vector (Clontech, 632164). The resultant plasmid was designated pLVX-lncPSCA. To test the protein-coding potential of *lncPSCA*, we synthesized the CPAT-predicted ORF (435–1,004 nt of NR_033343.2) and the "so-called" 5'UTR plus ORF (1–1,004 nt of NR_033343.2) (Genewiz) and, then, cloned them into the pEGFP-N1 vector. The two constructs were named as pEGFP-N1-ORF and pEGFP-N1-5'UTR-ORF. All these plasmids were sequenced to confirm the orientation and integrity.

CRISPR/Cas9-engineered *lncPSCA*-knockout cells

Considering *lncPSCA* shares exon 2 and exon 3 with the protein-coding *PSCA* gene, we designed two guide RNAs (gRNAs) covering the entire *lncPSCA* specific exon1 via targeting the 5'-flanking region (lncP-gRNA1) and the intron 1 (lncP-gRNA2) using Optimized CRISPR Design (Appendix Fig S6A and B and Appendix Table S5). The U6 promoter vector PX458M with two gRNA-expressing cassettes was developed from the vector PX458 which is also known as pSpCas9(BB)-2A-GFP with Cas9 from *S. pyogenes* with 2A-EGFP (Addgene, 48138). Firstly, lncP-gRNA1 was cloned into *Bbs*I digested PX458M (PX458M-lncP-gRNA1) and lncP-gRNA2 was cloned into *Bbs*I digested EZ-GuideXH (Life science market, PVT13420) (EZ-GuideXH-lncP-gRNA2). After both plasmids were digested with *Xho*I and *Hind*III, the digested DNA fragments were purified. The lncP-gRNA2 DNA fragment from the EZ-GuideXH-lncP-gRNA2 plasmid was then ligated to the digested PX458M-lncP-gRNA1 plasmid. The resultant plasmid with two *lncPSCA* gRNAs, designated PX458M-lncP-2gRNA, was sequenced to confirm the integrity. After transfected with PX458M-lncP-2gRNA or PX458M for 48 h, GFP-positive HGC-27 and MGC80-3 cells were selected by flow cytometry FACSAria II (BD, US) and seeded in 96-well culture plates. Multiple single cell clones were selected and cultured individually in separate wells. After genomic DNA was extracted from each cell clone, the deletion of *lncPSCA* exon1 was examined through PCR and Sanger sequencing with specific primers (Appendix Table S5).

Lentiviral transduction

Recombinant lentiviral particles were produced by transient co-transfection of the pLVX-lncPSCA, psPAX2 (Addgene, #12260) and pMD2.G (Addgene, #12259) plasmids into HEK293T cells. At 48 h and 72 h after transfection, viral supernatants were collected and filtered. Lentiviral particles harboring the *DDX5* shRNA or negative control shRNA were products of Genechem (35605-1, Shanghai, China) (Appendix Table S5). HGC-27 or MGC80-3 cells were infected with viral supernatant containing 5 μg/ml polybrene and then selected using 2 mg/ml puromycin. In these lentiviral transducted cells, expression of *lncPSCA* and *DDX5* was examined by RT–qPCR and/or Western blot.

Cell proliferation analyses

For transient transfection, a total of 1×10^4 HGC-27 or MGC80-3 cells were seeded in 12-well plates and then transfected with 0.5 μg pcDNA-lncPSCA, 0.5 μg pcDNA3.1, 20 nmol/l lncPSCA siRNAs (silncP-1 and silncP-2), 20 nmol/l *DDX5* siRNAs (siDDX5-1 and siDDX5-2), or 20 nmol/l NC RNA, respectively. Cells were harvested and counted at 24, 48, and 72 h after transfection. For the CRISPR/Cas9-engineered *lncPSCA*-knockout HGC-27 or MGC80-3 cells or cells with lentiviral transduction of overexpressed *lncPSCA* or the *DDX5* shRNA, 3×10^4 cells were seeded in 12-well plates. Cells were harvested and counted at 24, 48, and 72 h after seeding.

Colony formation assays

HGC-27 or MGC80-3 (2,000 cells per well) were seeded into a 6-well cell culture plate and transfected with indicated small RNAs or plasmids, respectively. The CRISPR/Cas9-engineered *lncPSCA*-knockout HGC-27 or MGC80-3 cells or cells stably transfected with the lncPSCA plasmid and the *DDX5* shRNA (2,000 cells per well) were seeded into a 6-well culture plate. When colonies were visible after 14 days, cells were washed with cold PBS twice and fixed with the fixation fluid (methanol:acetic acid = 3:1). After cells were dyed with crystal violet, the colony number in each well was counted.

Xenograft study

To examine the *in vivo* anticancer role of *lncPSCA*, we inoculated subcutaneously a total of 5×10^6 various HGC-27 cells (WT, wild type; KO-C14; KO-C40) or MGC80-3 cells (WT; KO-C1; KO-C3) into fossa axillaris of five-week-old female nude BALB/c mice (Vital River Laboratory, Beijing, China) (HGC-27: $n = 7$ per group; MGC80-3: $n = 8$ per group). The mice were randomly assigned to different groups. Tumor growth was measured every three days after tumor volumes equaled to or were greater than 90 mm³. During *in vivo* metastasis analyses, a total of 2×10^6 various HGC-27 cells with stable firefly luciferase expression (WT, wild type; KO-C14; KO-C40) or MGC80-3 cells with stable firefly luciferase expression (WT; KO-C1; KO-C3) were given to mice via intravenous injection. Bioluminescent GC metastasis were monitored weekly via the IVIS Spectrum In Vivo Imaging System (PerkinElmer, USA). All procedures involving mice were approved by the institutional review aboard of Shandong Cancer Hospital and institute. All analysis was performed in a blinded fashion with individuals unaware of types of GC xenografts.

Immunohistochemistry (IHC)

Gastric cancer xenografts and mice lungs with metastasis tumors were formalin fixed, paraffin-embedded and stained with hematoxylin and eosin (HE). Histological detection of DDX5 (Millipore, 05-850) and Ki67 (Abcam, ab15580) was carried out following the standard protocol.

Wound healing and transwell assays

For wound-healing assays, a wound was scratched by a 10 μl pipette tip when the cell layer of HGC-27 or MGC80-3 reached about 90% confluence. Cells were continued cultured at 37°C with 5%

CO_2, and the average extent of wound closure was quantified. In transwell assays, the transwell chambers were coated with 60 µl BD Biosciences Matrigel (1:20 dilution) for 12 h in a cell incubator. HGC-27 and MGC80-3 cells were added to upper transwell chambers (pore 8 mm, Corning). A medium containing 10% FBS (650 µl) was added to the lower wells. After 48 h, cells migrated to the lower wells through pores were stained with 0.2% crystal violet solution and counted.

Subcellular fractionation

The cytosolic and nuclear fractions of HGC-27 or MGC80-3 cells were separately isolated using the nuclear/cytoplasmic Isolation Kit (Biovision, K266) according to the manufacturer's instructions.

RNA pull-down

LncPSCA was amplified by PCR from pcDNA-lncPSCA and cloned into a modified pMD19-T vector (TaKaRa) with inserted T7 promoter before and after the TA cloning site to prepare a plasmid construct as the template for *in vitro* RNA synthesis. The constructs were linearized and transcribed with T7 RNA polymerase (MEGAscript T7 Transcript Kit, Thermo fisher, AM1330). Sense and antisense lncPSCA were biotinylated with Pierce™ RNA 3' End Desthiobiotinylation Kit (Thermo, 20163) and incubated with HGC-27 nucleus extracts and Streptavidin magnetic beads at 4°C for 1 h. After beads were washed for three times, proteins bound were recovered with Elution Buffer following the instruction of Pierce™ Magnetic RNA-Protein Pull-Down Kit (Thermo, 20164). The retrieved proteins were then analyzed by Mass Spectrometry (Hoogen Biotech Co., Shanghai, China) and Western Blot. Eluted proteins were identified with the liquid chromatography–tandem mass spectrometry (LS-MS/MS) approach. Mass spectra were analyzed using MaxQuant software (version 1.5.3.30) with the UniProtKB human database (uniport *Homo sapiens* 188441_20200326).

RNA immunoprecipitation (RNA-IP)

RNA-IP assays were performed using the Magna RIP RNA-Binding Protein Immunoprecipitation Kit (Millipore, 17-700) with the DDX5 antibody (Millipore, 05-850) or IgG Isotype-control (Invitrogen, 02-6502). The DDX5-RNA complexes were then recovered by Dynabeads® Protein G beads. LncPSCA RNA levels in the precipitates were measured by RT–qPCR. A total of 10% of inputs were used for RT–qPCR.

Co-Immunoprecipitation (Co-IP)

Co-IP was performed between DDX5 and RNA Pol II. Gastric cancer cells were lysed in the lysis buffer containing 20 mmol/l Tris–HCl (pH 8.0), 10 mmol/l NaCl, 1 mmol/l EDTA (pH 8.0), 0.5% NP-40, and cOmplete™ Mini protease inhibitor (Roche, 11836170001). Cell lysates were incubated with antibodies of DDX5 (Millipore, 05-850) and RNA pol II (Millipore, 05-623) or control IgG (Invitrogen, 02-6502) overnight at 4°C and with Dynabeads® Protein G beads (Invitrogen, 10004D) at the next day for 2 h at 4°C. The beads were washed for five times with the lysis buffer, followed by Western blot. A total of 1% of inputs were used for Western blot.

Turnover assays

HGC-27 and MGC80-3 cells with stable overexpression of *lncPSCA* or knockout of *lncPSCA* were seeded in a 6 cm cell culture plate. After 24 h, cycloheximide (CHX) was added into the media at a final concentration of 60 µg/ml. The GC cells were harvested at the indicated times after CHX treatment. The DDX5 and GAPDH protein levels were analyzed by Western blot.

Ubiquitination assays

Ubiquitination assays were carried out in HEK293T and HGC-27 cells. In HEK293T cells, HA-ubi and Flag-DDX5 were cotransfected with the pcDNA3.1 vector or the pcDNA-lncPSCA plasmid as indicated. At 24 h after transfection, the cells were treated with 50 µg/ml MG132 for 6 h and then lysed with the IP lysis buffer (Beyotime, P0013). Proteins in the cell lysate were immunoprecipitated to isolate ubiquitinated DDX5, which was detected with the anti-HA antibody (Appendix Table S6). In HGC-27 cells, ubiquitinated DDX5 was isolated with the anti-DDX5 antibody (Millipore, 05-850) and endogenous ubiquitin chains on DDX5 were detected.

RNA-seq

To gain insight into how lncPSCA or DDX5 regulate gene expression in GC cells, we performed RNA-seq of HGC-27 cells transfected or transduced with different expression constructs. Total RNA was isolated from cultured cells using TRIzol. RNA-seq of HGC-27 cells transfected with pcDNA-lncPSCA was performed using Illumina HiSeq 2000 platform (Illumina, USA). RNA-seq of HGC-27 cells with stable expression of the *DDX5* shRNA was performed using BGISEQ-500 platform (BGI, Shenzhen, China). Sequenced reads were trimmed for adaptor sequence, and masked for low-complexity or low-quality sequence, then mapped to whole transcriptome using tophat2 or Bowtie2 with default parameters. Reads count of samples were calculated and converted to FPKM (fragments per kilobase of exon model per million reads mapped).

Statistics

The difference between two groups was calculated using Student's *t* test. One-way ANOVA analysis with Dunnett's test was used for multiple comparisons. The significance of association between gene expression and rs2978980 genotypes or between different genes was calculated using Spearman's correlation. The Pearson chi-square test was employed for comparing categorical variables in various clinical parameters. A *P* value of < 0.05 was used as the criterion of statistical significance. All analyses were performed with SPSS software package (Version 16.0, SPSS Inc.) or GraphPad Prism (Version 5, GraphPad Software, Inc.).

Data availability

The datasets produced in this study are available in the following databases: RNA-Seq data: Gene Expression Omnibus GSE145762 (https://www.ncbi.nlm.nih.gov/geo/query/acc.cgi?acc=GSE145762);

ChIP-seq and RNA-seq data: Gene Expression Omnibus GSE146431 (https://www.ncbi.nlm.nih.gov/geo/query/acc.cgi?acc=GSE146431).

Expanded View for this article is available online.

Author contributions

MY conceived and designed this study. YZ and MY acquired, analyzed, and interpreted the data from experiments. YZ, TL, GJ, HG, NZ, JC, MX, YX, TW, JL, YSong, BW, and JY were responsible for patient recruitment, biospecimen sampling, clinical data collection, and analysis. TL, GJ, HG, TW, YShen, and JY provided technique supports. YZ and HG were engaged in statistical and bioinformatics analyses. YZ and MY drafted the manuscript. MY critically revised the manuscript for important intellectual content. MY and JY supervised this study.

Conflict of interest

The authors declare that they have no conflict of interest.

References

Abnet CC, Freedman ND, Hu N, Wang Z, Yu K, Shu X-O, Yuan J-M, Zheng W, Dawsey SM, Dong LM *et al* (2010) A shared susceptibility locus in PLCE1 at 10q23 for gastric adenocarcinoma and esophageal squamous cell carcinoma. *Nat Genet* 42: 764–767

Betts JA, Moradi Marjaneh M, Al-Ejeh F, Lim YC, Shi W, Sivakumaran H, Tropée R, Patch A-M, Clark MB, Bartonicek N *et al* (2017) Long noncoding RNAs CUPID1 and CUPID2 mediate breast cancer risk at 11q13 by modulating the response to DNA damage. *Am J Hum Genet* 101: 255–266

Budanov AV (2011) Stress-responsive sestrins link p53 with redox regulation and mammalian target of rapamycin signaling. *Antioxid Redox Signal* 15: 1679–1690

Cheok CF, Lane DP (2017) Exploiting the p53 pathway for therapy. *Cold Spring Harb Perspect Med* 7: a026310

Cho SW, Xu J, Sun R, Mumbach MR, Carter AC, Chen YG, Yost KE, Kim J, He J, Nevins SA *et al* (2018) Promoter of lncRNA gene PVT1 is a tumor-suppressor DNA boundary element. *Cell* 173: 1398–1412

Clark EL, Hadjimichael C, Temperley R, Barnard A, Fuller-Pace FV, Robson CN (2013) p68/DdX5 supports beta-catenin & RNAP II during androgen receptor mediated transcription in prostate cancer. *PLoS One* 8: e54150

Cui H, Tang M, Zhang M, Liu S, Chen S, Zeng Z, Shen Z, Song B, Lu J, Jia H *et al* (2019) Variants in the PSCA gene associated with risk of cancer and nonneoplastic diseases: systematic research synopsis, meta-analysis and epidemiological evidence. *Carcinogenesis* 40: 70–83

El-Deiry WS (2016) p21(WAF1) Mediates Cell-Cycle Inhibition, Relevant to Cancer Suppression and Therapy. *Cancer Res* 76: 5189–5191

Gao P, Xia J-H, Sipeky C, Dong X-M, Zhang Q, Yang Y, Zhang P, Cruz SP, Zhang K, Zhu J *et al* (2018) Biology and clinical implications of the 19q13 aggressive prostate cancer susceptibility locus. *Cell* 174: 576–589

Guo H, Ahmed M, Zhang F, Yao CQ, Li SiDe, Liang YI, Hua J, Soares F, Sun Y, Langstein J *et al* (2016) Modulation of long noncoding RNAs by risk SNPs underlying genetic predispositions to prostate cancer. *Nat Genet* 48: 1142–1150

He W, Liang B, Wang C, Li S, Zhao Y, Huang Q, Liu Z, Yao Z, Wu Q, Liao W *et al* (2019) MSC-regulated lncRNA MACC1-AS1 promotes stemness and chemoresistance through fatty acid oxidation in gastric cancer. *Oncogene* 38: 4637–4654

Helgason H, Rafnar T, Olafsdottir HS, Jonasson JG, Sigurdsson A, Stacey SN, Jonasdottir A, Tryggvadottir L, Alexiusdottir K, Haraldsson A *et al* (2015) Loss-of-function variants in ATM confer risk of gastric cancer. *Nat Genet* 47: 906–910

Hu N, Wang Z, Song X, Wei L, Kim BS, Freedman ND, Baek J, Burdette L, Chang J, Chung C *et al* (2016) Genome-wide association study of gastric adenocarcinoma in Asia: a comparison of associations between cardia and non-cardia tumours. *Gut* 65: 1611–1618

Hua JT, Ahmed M, Guo H, Zhang Y, Chen S, Soares F, Lu J, Zhou S, Wang M, Li H *et al* (2018) Risk SNP-mediated promoter-enhancer switching drives prostate cancer through lncRNA PCAT19. *Cell* 174: 564–575

Huang JZ, Chen M, Chen D, Gao XC, Zhu S, Huang H, Hu M, Zhu H, Yan GR (2017) A peptide encoded by a putative lncRNA HOXB-AS3 suppresses colon cancer growth. *Mol Cell* 68: 171–184

ICGC/TCGA Pan-Cancer Analysis of Whole Genomes Consortium (2020) Pan-cancer analysis of whole genomes. *Nature* 578: 82–93

Kruiswijk F, Labuschagne CF, Vousden KH (2015) p53 in survival, death and metabolic health: a lifeguard with a licence to kill. *Nat Rev Mol Cell Biol* 16: 393–405

Leucci E (2018) Cancer development and therapy resistance: spotlights on the dark side of the genome. *Pharmacol Ther* 189: 22–30

Leucci E, Vendramin R, Spinazzi M, Laurette P, Fiers M, Wouters J, Radaelli E, Eyckerman S, Leonelli C, Vanderheyden K *et al* (2016) Melanoma addiction to the long non-coding RNA SAMMSON. *Nature* 531: 518–522

Liu HT, Liu S, Liu L, Ma RR, Gao P (2018) EGR1-mediated transcription of lncRNA-HNF1A-AS1 promotes cell-cycle progression in gastric cancer. *Cancer Res* 78: 5877–5890

Lochhead P, Frank B, Hold GL, Rabkin CS, Ng MTH, Vaughan TL, Risch HA, Gammon MD, Lissowska J, Weck MN *et al* (2011) Genetic variation in the prostate stem cell antigen gene and upper gastrointestinal cancer in white individuals. *Gastroenterology* 140: 435–441

Mocellin S, Verdi D, Pooley KA, Nitti D (2015) Genetic variation and gastric cancer risk: a field synopsis and meta-analysis. *Gut* 64: 1209–1219

Moradi Marjaneh M, Beesley J, O'Mara TA, Mukhopadhyay P, Koufariotis LT, Kazakoff S, Hussein N, Fachal L, Bartonicek N, Hillman KM *et al* (2020) Non-coding RNAs underlie genetic predisposition to breast cancer. *Genome Biol* 21: 7

Nyamao RM, Wu J, Yu L, Xiao X, Zhang FM (2019) Roles of DDX5 in the tumorigenesis, proliferation, differentiation, metastasis and pathway regulation of human malignancies. *Biochim Biophys Acta Rev Cancer* 1871: 85–98

Pan W, Liu L, Wei J, Ge Y, Zhang J, Chen H, Zhou L, Yuan Q, Zhou C, Yang M (2016) A functional lncRNA HOTAIR genetic variant contributes to gastric cancer susceptibility. *Mol Carcinog* 55: 90–96

Pan W, Zhang N, Liu W, Liu J, Zhou L, Liu Y, Yang M (2018) The long noncoding RNA GAS8-AS1 suppresses hepatocarcinogenesis by epigenetically activating the tumor suppressor GAS8. *J Biol Chem* 293: 17154–17165

Ploner C, Kofler R, Villunger A (2008) Noxa: at the tip of the balance between life and death. *Oncogene* 27(Suppl 1): S84–S92

Plummer M, Franceschi S, Vignat J, Forman D, de Martel C (2015) Global burden of gastric cancer attributable to Helicobacter pylori. *Int J Cancer* 136: 487−490

Rao S, Huntley M, Durand N, Stamenova E, Bochkov I, Robinson J, Sanborn A, Machol I, Omer A, Lander E *et al* (2014) A 3D map of the human genome at kilobase resolution reveals principles of chromatin looping. *Cell* 159: 1665−1680

Saeki N, Ono H, Yanagihara K, Aoyagi K, Sasaki H, Sakamoto H, Yoshida T (2015) rs2294008T, a risk allele for gastric and gallbladder cancers, suppresses the PSCA promoter by recruiting the transcription factor YY1. *Genes Cells* 20: 382−391

Saeki N, Saito A, Choi IJ, Matsuo K, Ohnami S, Totsuka H, Chiku S, Kuchiba A, Lee YS, Yoon KA *et al* (2011) A functional single nucleotide polymorphism in mucin 1, at chromosome 1q22, determines susceptibility to diffuse-type gastric cancer. *Gastroenterology* 140: 892−902

Sakai S, Ohhata T, Kitagawa K, Uchida C, Aoshima T, Niida H, Suzuki T, Inoue Y, Miyazawa K, Kitagawa M (2019) Long noncoding RNA ELIT-1 acts as a Smad3 cofactor to facilitate TGFbeta/Smad signaling and promote epithelial-mesenchymal transition. *Cancer Res* 79: 2821−2838

Sakamoto H, Yoshimura K, Saeki N, Katai H, Shimoda T, Matsuno Y, Saito D, Sugimura H, Tanioka F *et al* (2008) Genetic variation in PSCA is associated with susceptibility to diffuse-type gastric cancer. *Nat Genet* 40: 730−740

Shi Y, Hu Z, Wu C, Dai J, Li H, Dong J, Wang M, Miao X, Zhou Y, Lu F *et al* (2011) A genome-wide association study identifies new susceptibility loci for non-cardia gastric cancer at 3q13.31 and 5p13.1. *Nat Genet* 43: 1215−1218

Statello L, Guo CJ, Chen LL, Huarte M (2021) Gene regulation by long non-coding RNAs and its biological functions. *Nat Rev Mol Cell Biol* 22: 96−118

Sung H, Ferlay J, Siegel RL, Laversanne M, Soerjomataram I, Jemal A, Bray F (2021) Global cancer statistics 2020: GLOBOCAN estimates of incidence and mortality worldwide for 36 cancers in 185 countries. *CA Cancer J Clin* 71: 209−249

Sung H, Yang HH, Hu N, Su H, Taylor PR, Hyland PL (2016) Functional annotation of high-quality SNP biomarkers of gastric cancer susceptibility: the Yin Yang of PSCA rs2294008. *Gut* 65: 361−364

Tanikawa C, Kamatani Y, Toyoshima O, Sakamoto H, Ito H, Takahashi A, Momozawa Y, Hirata M, Fuse N, Takai-Igarashi T *et al* (2018) Genome-wide association study identifies gastric cancer susceptibility loci at 12q24.11-12 and 20q11.21. *Cancer Sci* 109: 4015−4024

Wang T, Zhang L, Li H, Wang B, Chen K (2012) Prostate stem cell antigen polymorphisms and susceptibility to gastric cancer: a systematic review and meta-analysis. *Cancer Epidemiol Biomarkers Prev* 21: 843−850

Wang X, Liang Q, Zhang L, Gou H, Li Z, Chen H, Dong Y, Ji J, Yu J (2019) C8orf76 promotes gastric tumorigenicity and metastasis by directly inducing lncRNA DUSP5P1 and associates with patient outcomes. *Clin Cancer Res* 25: 3128−3140

Wang Z, Dai J, Hu N, Miao X, Abnet CC, Yang M, Freedman ND, Chen J, Burdette L, Zhu X *et al* (2017) Identification of new susceptibility loci for gastric non-cardia adenocarcinoma: pooled results from two Chinese genome-wide association studies. *Gut* 66: 581−587

Xu TP, Ma P, Wang WY, Shuai Y, Wang YF, Yu T, Xia R, Shu YQ (2019) KLF5 and MYC modulated LINC00346 contributes to gastric cancer progression through acting as a competing endogenous RNA and indicates poor outcome. *Cell Death Differ* 26: 2179−2193

Yan C, Zhu M, Ding Y, Yang M, Wang M, Li G, Ren C, Huang T, Yang W, He B *et al* (2020) Meta-analysis of genome-wide association studies and functional assays decipher susceptibility genes for gastric cancer in Chinese populations. *Gut* 69: 641−651

Zhang E, He X, Zhang C, Su J, Lu X, Si X, Chen J, Yin D, Han L, De W (2018a) A novel long noncoding RNA HOXC-AS3 mediates tumorigenesis of gastric cancer by binding to YBX1. *Genome Biol* 19: 154

Zhang J-X, Chen Z-H, Chen D-L, Tian X-P, Wang C-Y, Zhou Z-W, Gao Y, Xu YI, Chen C, Zheng Z-S *et al* (2018b) LINC01410-miR-532-NCF2-NF-kB feedback loop promotes gastric cancer angiogenesis and metastasis. *Oncogene* 37: 2660−2675

Zhang M, Weng W, Zhang Q, Wu Y, Ni S, Tan C, Xu M, Sun H, Liu C, Wei P *et al* (2018c) The lncRNA NEAT1 activates Wnt/beta-catenin signaling and promotes colorectal cancer progression via interacting with DDX5. *J Hematol Oncol* 11: 113

Zhang N, Li Y, Xie M, Song Y, Liu J, Lei T, Shen Y, Yu J, Yang M (2020) DACT2 modulated by TFAP2A-mediated allelic transcription promotes EGFR-TKIs efficiency in advanced lung adenocarcinoma. *Biochem Pharmacol* 172: 113772

Zhu M, Yan C, Ren C, Huang X, Zhu X, Gu H, Wang M, Wang S, Gao Y, Ji Y *et al* (2017) Exome array analysis identifies variants in SPOCD1 and BTN3A2 that affect risk for gastric cancer. *Gastroenterology* 152: 2011−2021

Zhuo W, Liu Y, Li S, Guo D, Sun Q, Jin J, Rao X, Li M, Sun M, Jiang M *et al* (2019) Long noncoding RNA GMAN, up-regulated in gastric cancer tissues, is associated with metastasis in patients and promotes translation of Ephrin A1 by competitively binding GMAN-AS. *Gastroenterology* 156: 676−691